Pressure dependence of low-frequency zero-sound propagation in superfluid ^{3}He-A and -A_1

R. F. Berg* and G. G. Ihas

Department of Physics, University of Florida, Gainesville, Florida 32611

(Received 19 February 1985)

The attenuation of low-frequency (5 MHz) zero sound in the A and A_1 phases of ^{3}He has been measured for pressures ranging from 2 to 31 bars, temperatures near T_c, and the $\hat{l}$ texture perpendicular to $\hat{q}$, the sound vector. These parameters are anticipated to allow the most valid comparison possible with the simple, collisionless theory using the Ginzburg-Landau description of the order parameter. The magnitude of the attenuation maximum agrees with theory at all pressures if the theoretical result is divided by 4. Its position agrees with theory only at low pressure. The sound velocity measured in the A phase from 9 to 31 bars scales approximately according to the theory. The velocity for T such that $\hbar\omega = 2\Delta$ is not equal to that at T_c, as predicted. The results do not depend on the magnitude of the applied magnetic field in the range 14 to 42 mT. Coupled with ancillary measurements, the determination of the NMR frequency of the sample of helium under study provided very precise, *in situ* thermometry.

I. INTRODUCTION

More than a decade of experimental study of the ^{3}He superfluids has firmly established their connection to the theoretical models of Anderson, Brinkman, and Morel (ABM) and Balian and Werthamer (BW);[1] these models, nevertheless, have not led to a complete understanding of the ordered liquid states. This is partly because the appropriate experimental facilities are not much more numerous than high-energy accelerators and partly because of the inherent complexity of the superfluids as reflected in their models. This complexity often requires a combination of design considerations such as sample shape and history not found in other condensed-matter experiments. Otherwise, complicated or perhaps impossible numerical calculations may be necessary to analyze experimental results.

We report here an experimental ultrasound study of ^{3}He-A in which magnetic field strength and direction and ultrasound frequency were chosen to enable a direct connection to the most analytically simple form of the theory for zero sound dispersion in ^{3}He-A at all liquid pressures. This theory, whose earliest forms are due to Serene[2] and Wölfle,[3] has its most detailed published exposition in Wölfle's 1978 review chapter.[4] The features of zero sound dispersion which have been experimentally verified include attenuation peaks caused both by breaking of Cooper pairs and by excitation of various vibrational modes of the tensor order parameter as well as accompanying velocity changes. Simplification of the general theory can occur in several ways. The most important is a choice of sound frequency ω much faster than the quasiparticle collision time τ, namely $\omega\tau \gg 1$. However, it can also be useful to keep the frequency sufficiently low so that the sound quantum $\hbar\omega$ is small compared to the superfluid transition temperature: $\hbar\omega \ll k_B T_c$. Figure 1 shows the frequency regime bounded by these requirements as a function of pressure. Our choice of 5 MHz for this study is a compromise for the entire liquid pressure range.

Low-frequency (5—10 MHz) zero sound has also the advantages that the order-parameter excitations occur very near T_c, allowing a simple Ginzburg-Landau description of the gap magnitude, and also yielding attenuation maxima at low pressures which are not too high for observation by a cell transit method.

With the above frequency restrictions assumed, it is possible to numerically evaluate an expression for the collisionless sound dispersion in terms of the cosine of the angle between the sound vector $\hat{q}$ and the order-parameter gap axis $\hat{l}$. We applied magnetic fields of 14.3, 28.6, and 42 mT to our sample parallel to $\hat{q}$. Since our measurements were within 2% of T_c, this forced $\hat{l}$ to lie perpendicular to $\hat{q}$ almost everywhere, the only uniform orientation available in a bulk geometry.

In addition to simplifying the superfluid texture, the magnetic field was important in two other ways. Most
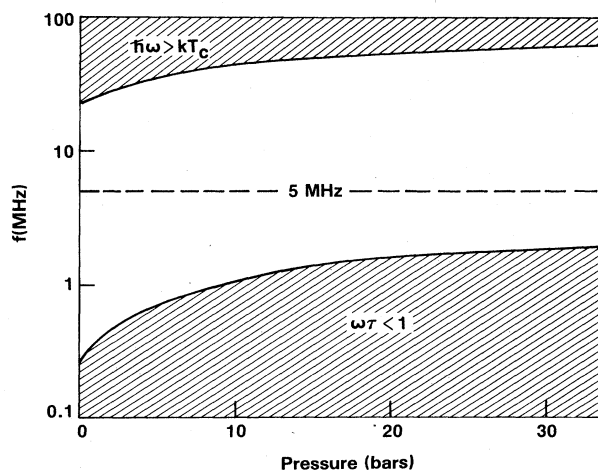

FIG. 1. Pressure-dependent frequency window for "simple" zero-sound measurements. $\tau T^2 = 4 \times 10^{-12}$ sec K^2 is assumed.

importantly, it allowed observation of the stabilized A phase at arbitrarily low pressures even though its width was as little as 20 μK at the lowest pressure. Secondly, the field allowed us to exploit the NMR shift inherent to the superfluid for precise, *in situ* thermometry for the sound measurements.

Some of the earliest investigations of superfluid ^{3}He-A used 5, 15, and 25 MHz ultrasound.[5,6] In 1975, Ketterson et al.[7] reported a series of 20-MHz sound measurements between 17 and 28 bars. The measurements of Paulson et al.[8] in 1977 yielded 5-MHz measurements at 24 and 33 bars that were especially useful for comparison against our own. More recently, Avenel et al.[9] inferred the temperature location of the 14.7-MHz clapping peak at 0.37 bar from attenuation data in its vicinity.

Our A-phase sound measurements are the first to cover essentially all of the liquid pressure range and thus give new comparisons against the relevant theory. Sections II and III of this paper cover the experimental apparatus and technique used for these measurements. Section IV describes how the experimental data were reduced, with an emphasis on our practical use of the superfluid NMR shift as a thermometer.

The results of this series of measurements are given in Sec. V chiefly in comparison against the collisionless theory of sound dispersion in the superfluid A phase. The amplitudes of the peak attenuations and the velocity drops scale according to the predictions of this theory but, especially at the higher pressures, the temperature locations of the attenuation peaks are colder than predicted.

II. APPARATUS

Our nuclear adiabatic demagnetization stage consisted of 60 moles of copper in the field of a commercial 8-T niobium-titanium magnet. A homemade dilution refrigerator precooled this copper bundle through an indium heat switch. A heat exchanger, consisting of 0.07 μm silver powder pressed into concentric annular cavities in a block of oxygen-free high-conductivity copper with no heat treatment, provided thermal contact between the ^{3}He sample and the copper bundle. At temperatures below a few millikelvin, the dominant thermal resistance in this system was due to the long copper nuclei-lattice coupling time so that our residual heat leak of 3 nW allowed a minimum temperature of 0.4 mK. For about the first month after cooldown an additional heat leak was present whose magnitude and time dependence suggested the ortho-para conversion of 3×10^{-4} moles of hydrogen, about 7% of the amount of exchange gas we used for the initial cooldown.

The refrigerator cooled about $\frac{1}{2}$ mole of liquid ^{3}He contained in the heat exchanger, a bellows pump, and the beryllium-copper sound cell. Figure 2 shows the assembled contents of the sound cell, consisting chiefly of machined epoxy pieces (Stycast 1266, Emerson and Cuming).

The fraction of the total ^{3}He sample actually probed by the sound and NMR was only about 1%. Sound pulses were transmitted and received by the two 9.5-mm-diam, 5-MHz, gold-plated X-cut quartz piezoelectric transduc-
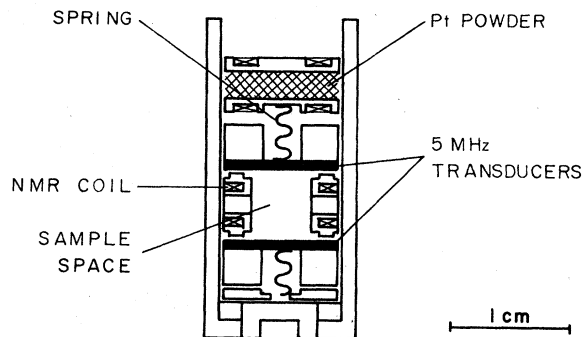

FIG. 2. Cross section through the contents of the sound cell. The cold sound path length of 6.25 mm is defined by the cylindrical epoxy spacer on which the ^{3}He NMR coil is wound.

ers separated by a cylindrical spacer. Ground connections to the transducers' inner faces were made via silver paint coating the ends of the spacer. Electrical connections to the opposite faces of the transducers were made by light, nonmagnetic springs, which also held the transducers in place against the spacer. A small amount of indium solder held a connecting wire (not shown) to the end of each spring.

The machined epoxy spacer defined the sound path length (6.25±0.05 mm) and diameter (5.0 mm). Some 23 mm^2 of radial holes, including those created by the crenelations at the spacer ends, provided thermal-conduction paths for the helium inside. In order to perform NMR measurements on the same sample probed by the sound, a flattened saddle-shaped rf coil was wound on grooves cut into the spacer. The location of this coil is the reason that the more usual choice of metal or quartz for a spacer material was not made. The coil's orientation places it perpendicular to the static field.

One interesting note is that a naive calculation of the eddy current heating induced in the nearby gold transducer coating can give a value as high as many nanowatts at the rf levels and frequencies routinely used in this experiment. Apparently the details of the rf field configuration and its intersection with the gold film prevent such a disaster from occurring. The heating seen at rf currents 10 times that ordinarily used was less than or on the order of 1 nW.

A second rf coil wound on a tube containing platinum powder for thermometry was not used in this experiment. The other machined epoxy pieces are a spring backing plate and annular cylinders designed to reduce the sound cell volume.

Pressure measurement and control were effected by using a capacitive strain gauge coupled by an electronic scheme to a bellows pump. The sensitivity of the pressure transducer was about 10^{-4} bars and worked well up to 36 bars. The settings of the ratio transformer for the strain gauge were related to the sample pressure through calibrations made against a 1500-psi (103 bars) Heise Bourdon pressure gauge. The resulting data were fit to a second-order polynomial with an rms deviation of less than 0.01 bar, which is more than the estimated inaccuracy of the

Heise gauge obtained from ^{3}He melting curve comparisons at the nuclear ordering temperature (1.0 mK) and at the melting curve minimum pressure (318 mK).

The dependence of sound velocity on pressure imposes a requirement on the stability of the pressure during a single run where changes in phase velocity are measured. A velocity precision of $\Delta c/c \sim 10^{-5}$ requires $\Delta P \sim 10^{-4}$ bars in the region where $(dc/dP)/c$ is greatest. The stability of the pressure regulation, as estimated by observation of an independent volume transducer, indicated that this requirement was met.

Magnetic fields applied to this experiment were created by a system of superconducting coils contained within the vacuum jacket and attached to the mixing chamber. The portion of this system pertinent to this experiment consisted of a main vertical Helmholtz coil, its associated flux transformer (cf. below), a horizontal gradient coil, and the room-temperature driving electronics. Fields of 14, 28, and 42 mT were persisted in the vertical coil pair with a homogeneity in the NMR region of $\Delta B/B = 4 \times 10^{-4}$. The horizontal gradient coil was used to enhance the amplitude of the NMR peak. Its effect on the overall field homogeneity or central field value was negligible.

Built into the circuit of the vertical coil is the secondary winding of a flux transformer. This field sweeping system[10] gives the advantages of higher precision and less ambiguity due to flux exclusion by the main coil compared to the more usual method of sweeping with an independent coil. A power operational amplifier (BOP 36-5M, Kepco) configured for voltage-controlled current output drove the primary winding of the flux transformer. A homemade 12-bit digital ramp programmed the operational amplifier with a triangular sweep pattern and provided the trigger pulse for starting data acquisition by the digital oscilloscope.

NMR absorption spectra were obtained at a constant frequency (0.4 to 1.4 MHz) while making small sweeps of the magnetic field about resonance. The detector, a high-frequency lock-in amplifier (Princeton Applied Research model No. 5202), measured the output of an rf canceling circuit as outlined in Fig. 3.
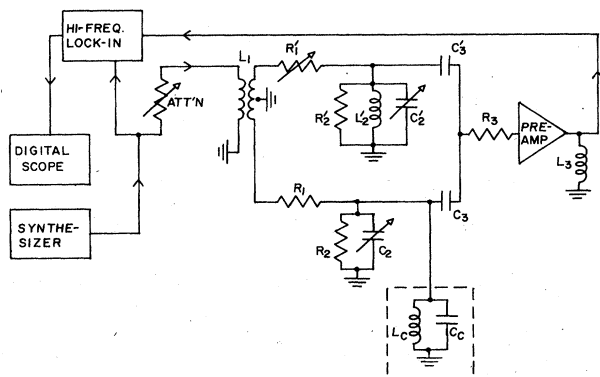
The particulars of this bridge circuit are as follows. After attenuation to the desired voltage level, an rf synthesizer (General Radio model No. 1163-A) drives the primary of a center-tapped rf transformer (Mini-Circuits model No. MCL T4-1). The resulting two outputs, differing by 180°, drive approximately symmetric LC tuned circuits through the large resistances R_1 and R'_1 (~ 100 kΩ). The net voltage is coupled by C_3 and C'_3 (22 pF) to the low-noise preamplifier (Analog Modules model No. LNVA-V) and then detected. The resistance R_3 (120 Ω) is necessary to kill parasitic oscillations of the preamp and L_3 (1 μH) blocks 60-Hz variations of the preamp output. Tuning is accomplished by first setting C_2 to give the Larmor resonant frequency in the cryostat coil and then adjusting the dummy-circuit component (primed) values to null the bridge output. While extinction ratios as small as 10^{-4} were possible, tuning stability typically limited these values to $\sim 10^{-3}$. This bridge scheme reduced the effect of noise from the lock-in which would have otherwise been important due to the lock-in's limited dynamic range. The vector sum of the in-phase and quadrature signals is the final analog output of the spectrometer.

The electronic system used for sound measurements is illustrated by Fig. 4. It consists of means for sending a short sound burst through the liquid helium and then detecting, amplifying, and processing this burst to obtain either attenuation or phase velocity change information about the medium of propagation. A 5-MHz synthesizer's output (Hewlett-Packard model No. 3325A) is gated and amplified by a Matec 310HP, which is triggered at 30 Hz synchronously with the 125 V ac line. The resulting output, 10 cycle bursts of 5 MHz rf coherent with the pulse envelope, drives the transmitting quartz crystal after attenuation to a peak-to-peak amplitude of 0.60 V. The signal induced in the receiving transducer is amplified first by a ham radio tuned preamplifier (Palomar model No. P-308) and then by a 200-MHz wideband amplifier (Matec model No. 625).
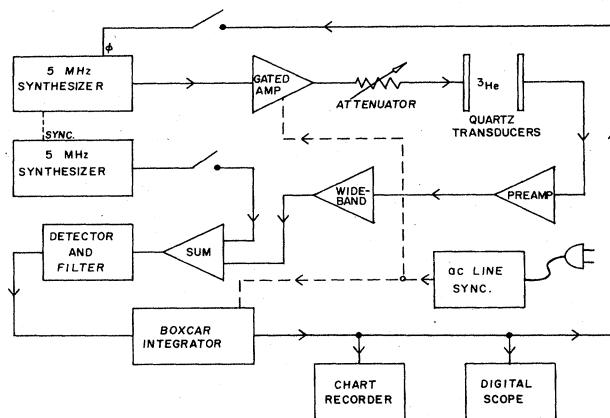

FIG. 3. Constant-frequency NMR detection scheme. Off balance signal of the rf bridge is detected by the high-frequency lock-in amplifier.

FIG. 4. Block diagram of 5-MHz ultrasound measurement using pulsed transmission across the ^{3}He cell. Closing the two switches changes the amplitude measurement mode into a phase detection mode where output to the recorders is the error signal of the phase-locked loop.

Different arrangements are then used to measure either attenuation or velocity. For measurements of attenuation, the amplified received pulse is detected and filtered at 500 kHz. A boxcar integrator (Princeton Applied Research model No. CW-1) using a gate width of about 2 μsec and gate delay of 20 to 30 μsec gives the average voltage of the received waveform in the vicinity of the waveform maximum. From this amplitude the attenuation of the ^{3}He relative to that at a reference temperature can be ascertained.

Changes in the phase velocity of the ^{3}He can be measured if the phase of the received rf pulse is compared against a stable reference (here, a PTS 200 synthesizer synchronized to the HP synthesizer). Simply summing the reference and the received signal will give an output which goes as the cosine of the angle between the two inputs. Unfortunately, for changes in the input phase difference of more than a few degrees, this cosine relation between output voltage and input phase is a nonlinear one and even gives zero sensitivity at the 0° and 180° points. However, by using feedback, the phase of the transmitted signal can be continuously adjusted to keep it near the most favorable point (in terms of phase sensitivity) in relation to the reference phase. Closing the two open switches in Fig. 4 adds the reference signal to the received pulse before detection and allows the boxcar output to become the error signal for the phase controlling input of the synthesizer. In the limit of high loop gain, the sensitivity of this scheme to changes in the phase of the received signal is simply equal to the phase programming coefficient of the helium signal synthesizer.

III. EXPERIMENTAL TECHNIQUES

Over the week or two following an initial gross demagnetization, minute step decreases in the bundle solenoid field were made one to four times per day to keep the nuclear stage in the vicinity of T_c. Although the temperature remained within 3% of T_c during this entire time, the bundle entropy was of course continuously increasing, with a resulting loss in heat capacity. When the temperature drift rate had risen to an unacceptably high level (or some other experimental contingency arose) the bundle was remagnetized to begin another cycle.

Data taking commenced after demagnetizing the bundle sufficiently to cool the ^{3}He to $\sim 0.99\,T_c$. After an equilibration time of ~ 30 min, the ^{3}He temperature drifted linearly up toward T_c over the next several hours. Points were accumulated above T_c to establish data baselines before stopping data acquisition. Calibrations of the sound signal were performed at least once at each pressure at just above T_c to obtain data reduction parameters.

Recording the information contained in the ^{3}He NMR and ultrasound signals included conversion of the analog signals to digital form and some on-line data reduction. The entire process repeated every two minutes as timed by the digital ramp sweeping the static NMR field at an amplitude of 10 to 40 μT. At the start of a sweep, a trigger signal sent by the ramp caused a two-channel signal averager (Nicolet model No. 1170, actually used only for analog to digital conversion) to begin recording the NMR

and ultrasound signals and then send this information to the computer (Hewlett-Packard model No. 9845A). After receiving the data, the computer found the highest NMR point and fitted a parabola to the neighboring points. The single number representing the fitted peak location was recorded. The sound data, simultaneously accumulated during the field sweep, were fit to a linear function of time $S(t)$ and the value of $S(t)$ at the time represented by the NMR peak location was recorded. Data files stored on magnetic cassette tapes thus consisted of up to 200 two-component entries taken at two-minute intervals.

The excitation voltage amplitude (0.60 V peak-to-peak) and duty cycle (2.0 μsec every $\frac{1}{30}$ sec) of the sound transducer were chosen as a compromise between heating and signal-to-noise ratio. For example, pulsing the transmitting transducer at a 6-Hz rate but at 15 V peak-to-peak caused some 30- to 60-nW heating at ~ 1.5 mK, 20.5 bars (normal liquid). Assuming that this heating is proportional to the input electronic power, the local heat leak due to the transducers during data collection was then some 0.2 to 0.5 nW.

The detected signal sent to the boxcar integrator consisted of a quickly decaying capacitive feedthrough pulse followed by the signal due to sound traversing the 6.25-mm-long cell. This was followed by further structure due to the coherent summation of successive echoes enabled by the ringing of the quartz transducers. The boxcar window was always placed in the vicinity of the first maximum to avoid effects due to following echoes and also to avoid interference by spurious feedthrough signals as much as possible. This feedthrough signal, a result of ringing in the receiver circuit caused by capacitive pickup of the electronic transmitter pulse, produced interference with the helium sound signal. The amplitude of the feedthrough signal was always only a few percent of the helium signal except at the superfluid attenuation maximum at 2.05 bars. The amplitude dependence of the phase-locked loop for the velocity measurement then became an important effect which produced artifacts in the data at that pressure.

IV. NMR THERMOMETRY AND DATA REDUCTION

For data reduction, each data file was examined and the point nearest T_{c1} was defined by its signature in the sound or NMR data. This point plus a second, warmer point, typically defined an hour later in the data, established a region of normal fluid data for baseline purposes. Reduction of the NMR and sound data then proceeded separately as described below and the sets of reduced data were afterward combined to give plots of sound dispersion versus temperature.

A. NMR thermometry

The discovery of large temperature-dependent NMR frequency shifts in the superfluid A phase,[11] besides stimulating much more experimental and theoretical work in that area, also gave promise that the ^{3}He sample itself could be used as a thermometer (e.g., see Ref. 12). To date this has not been done, perhaps because of a lack of cer-

tainty about the necessary calibration data. A few ancillary calibrations made in the course of these experiments support the theoretical picture of the magnitude of these shifts[13] as well as corroborate most of the existing NMR shift calibrations. The net result is a basis for thermometry in the A and A_1 phases accurate to $\sim 10\%$, but with a precision achieved in magnetic fields of modest homogeneity which is comparable to lanthanum-doped
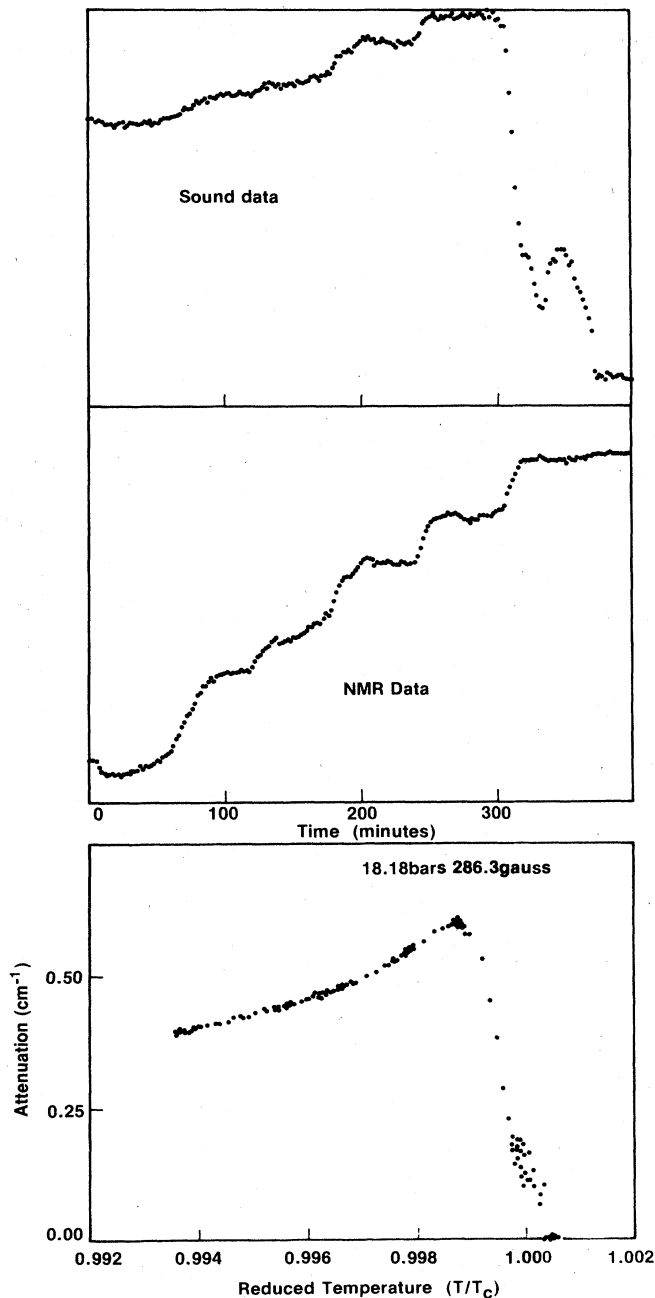

FIG. 5. Deconvolution of sound attenuation vs temperature from raw NMR frequency and sound-amplitude data. The irregular clustering of points in the attenuation plot is due to the strongly time-dependent heat leak of this example.

cerium magnesium nitrate (LCMN) thermometry. The real advantage is a truly *in situ* thermometer, as Fig. 5 illustrates. This shows the raw sound and NMR data on an unusual run badly disturbed by a time-dependent heat leak caused by a touch in one of the cryostat vibration isolation mounts. After deconvolution, the sound attenuation versus temperature data fall on a curve similar to those of quiet runs, but with an inhomogeneous data point distribution along that curve, where certain temperature regions were retraced due to heat spikes followed by cooling.

Obtaining temperature shifts from the NMR data starts with the knowledge that, for temperatures deep into the A phase [i.e., several A_1-phase widths ($T_{c1}-T_{c2}$) below the normal phase] the NMR frequency ω departs from the Larmor value γH according to

$$\omega^2 = (\gamma H)^2 + \Omega_A^2 \ . \tag{1}$$

Calculation of the shift in the NMR frequency has been done for the various unitary phases of superfluid ^{3}He by Leggett.[13] In general, the longitudinal frequency is a product of a function of pressure $f(P)$ and $(1-T/T_c)$,

$$\Omega_A^2 = (2\pi)^2 \nu_A^2 = (2\pi)^2 f(P)(1-T/T_c), \quad T < T_c \ , \tag{2}$$

where, for the ABM state,

$$f(P) = (\pi/10)\langle R^2 \rangle \gamma^2 N_F (1+F_0^a)[\ln(1.14\epsilon_c/k_B T_c)]^2$$
$$\times (k_B T_c)^2 (\Delta C/C_N) \ . \tag{3}$$

In Eq. (3), γ, N_F, and F_0^a are the gyromagnetic ratio, the density of states at the Fermi surface, and the $l=0$ antisymmetric Landau parameter, respectively. The quantity ϵ_c is an energy integral cutoff, estimated to be about 0.7 K by Leggett.[14] Most strong coupling effects are absorbed into the experimentally measured ratio of the jump in the heat capacity at T_c to the normal heat capacity $(\Delta C/C_N)$. Here $\langle R^2 \rangle$ is an angular average of the square of the quasiparticle renormalization factor and is on the order of unity.

Various determinations[15–18] of $f(P)$ are sufficiently dense between 20 and 34 bars to calibrate ^{3}He NMR thermometry at high pressures. However, since $f(P)$ decreases by an order of magnitude as the pressure is lowered from melting to zero pressure, this calibration cannot be accurately extrapolated to low pressures. Our measurement of $f(P)$ at 2.05 bars (Ref. 19) allows Eq. (2) to be used as an interpolation formula with $\langle R^2 \rangle$ as a single fit parameter. Further measurements[20] of $f(P)$ covering the entire liquid pressure range show that this interpolation formula has the required accuracy.

The nuclear-magnetic-resonance frequency also exhibits a shift in the A_1 phase which can be easily understood in terms of a Ginzburg-Landau description. Takagi[21] and Osheroff and Anderson[15] have discussed how the shift frequency ν_A depends on temperature by starting with the behavior of the two (different) order parameters for the up- and down-spin components for the liquid. It will be useful to define a new temperature scale linear in T but with its zero at T_{c2} and its degree equal to the width of the A_1 phase. We write

$$U = \frac{T_{c2} - T}{T_{c1} - T_{c2}} . \qquad (4)$$

The NMR shifts in the A_1 $(-1 < U < 0)$ and A $(0 < U)$ phases as a function of temperature can then be written in terms of two quantities, the products CA and CB in the equations below:

$$v_A^2 = \begin{cases} (C/4)A(1+U), & -1 < U < 0 & (5) \\ (C/4)[A + 2BU + 2(A + BU)^{1/2}(BU)^{1/2}], & 0 < U . & (6) \end{cases}$$

Deep into the A phase the shift can be well approximated by a linear form:

$$v_A^2 = (C/4)(2A + 4BU), \quad U > 1 . \qquad (7)$$

For NMR thermometry using v_A^2 in or near the A_1 phase, T_{c1}/T_c and T_{c2}/T_c, the two reduced transition temperatures, must be known. This is equivalent to knowing the width of the A_1 phase $(T_{c1} - T_{c2})/T_c$, and the asymmetry of T_{c1} and T_{c2} about T_c. This asymmetry can be written in terms of a Ginzburg-Landau parameter δ which measures the coupling of the up- and down-spin gaps:

$$\frac{T_{c1} - T_c}{T_{c2} - T_c} = -\frac{1+\delta}{1-\delta} . \qquad (8)$$

The ratio of the temperature derivatives of v_A^2 in the A_1 and deep in the A phase (a measurable quantity) is related to δ:

$$\frac{(d\, v_A^2/dT)_{A_1}}{(d\, v_A^2/dT)_A} = \frac{CA}{4CB} = \frac{1-\delta}{4} . \qquad (9)$$

To avoid confusion, we mention that this parameter δ is the same used in the two 1975 reviews of Ref. 1 and can be written in terms of three of the five generalized free-energy coefficients β_i as originally defined by Mermin and Stare,[22]

$$\delta = \frac{-(\beta_2 + \beta_4 + 2\beta_5)}{\beta_2 + \beta_4} . \qquad (10)$$

Before deconvoluting the temperature of the ^{3}He sample from the measured NMR shifts, two corrections for systematic errors had to be made. The first correction dealt with the uniform change in time of the NMR frequency caused by decay (3 mT/year) of one or both of the persisted solenoids in the cryostat. A baseline defined by a linear fit to the normal region just above T_{c1} was subtracted from all of the NMR data. The effects of a comparable relaxation change seen shortly after persisting the bundle solenoid were avoided by ignoring any data taken in a period of about an hour following the persistence of this solenoid.

The second correction dealt with discontinuities in the NMR data apparently caused by changes in the positions of large iron objects in the neighborhood of the cryostat. The data were corrected for these discontinuities simply by requiring continuity at the dislocation by adding an appropriate constant to all of the points later than the dislo-

cation. Such a healing process, required an average of about once every 10 h of data, was usually extremely successful as judged by the smooth appearance of the data afterwards.

After performing these systematic corrections, the magnitude of v_A^2 was calculated and the reduced temperature was obtained by inverting Eqs. (5) and (6):

$$U = \begin{cases} 4v_A^2/AC - 1, & 0 < v_A^2 < AC/4 & (11) \\ (4v_A^2 - AC)^2/16BCv_A^2, & AC/4 < v_A^2 & (12) \end{cases}$$

$$T/T_c = 1 - [(1-\delta)/2 + U](T_{c1} - T_{c2})/T_c . \qquad (13)$$

The quantities AC and BC in Eqs. (11) and (12) are

$$BC = f(P) \left[\frac{T_{c1} - T_{c2}}{T_c} \right] , \qquad (14)$$

$$AC = BC(1-\delta) . \qquad (15)$$

The value of the A-phase shift coefficient BC was obtained at each pressure by using Eqs. (2) and (3) with $\langle R^2 \rangle \equiv 0.70$. The melting curve values for δ and the magnetic-field-dependent quantity $(T_{c1} - T_{c2})/T_c$ obtained by Osheroff and Anderson[15] were used for all pressures. $(T_{c1} - T_{c2})/T_c = 0.024$ T^{-1} while, as defined by Leggett in Ref. 1, $\delta = 0.25$. The Helsinki temperature scale[23] was used for $T_c(P)$.

Recently two different groups of workers[24,25] have reported measurements of $(T_{c1} - T_{c2})$ and $(T_{c2} - T_c)$ over the entire liquid pressure range. Instead of remaining pressure independent as we had assumed, both δ and $(T_{c1} - T_{c2})/T_c$ were found to decrease with decreasing pressure, falling to 0% and 60% of their melting curve values, respectively, at zero pressure. The effect of these pressure dependences on our analysis was checked and found to be less than 1% in the region of the clapping maxima. This was expected since the NMR temperature scale quickly becomes insensitive to the choices of δ and $(T_{c1} - T_{c2})/T_c$ as one cools below the A_1 phase.

On each run the temperature drift $\dot{T}$ showed no discontinuity between the A and A_1 phases. This was at first surprising in light of the fact that the heat-capacity jump at T_c is split into approximately equal parts at T_{c1} and T_{c2} by a magnetic field.[26] However, the helium, with a heat capacity 1% that of the copper bundle, was sufficiently well coupled to the copper that the helium heat-capacity changes went unnoticed.

B. Sound amplitude and velocity

Sound-amplitude data were subtracted from a baseline defined as the average of the raw data in the same normal region span used to define the NMR baseline. Subsequent reduction of the data depended on whether velocity or attenuation data were handled.

The calibrations of the voltages representing attenuation were made by varying the sound drive by 3 dB when $T > T_c$ and assuming linearity. The exception to this procedure was for the 2-bars calibration, where the attenuation was sufficiently high that the nonlinearity of the measuring system became important. Here, the calibration was defined as the difference between the normal

operating value and that obtained with no transducer excitation whatsoever. This definition increased the accuracy of the high attenuation points at the expense of the lower attenuation points. Since the absolute attenuation was not measured, all measurements are referred to the attenuation at T_c.

Calibrations of the sound-velocity data were made in the limit of small sound-velocity changes Δc, where the relative sound-velocity change in a cell of length L is proportional to the shift in the received phase of the sound after crossing the cell:

$$\frac{\Delta c}{c} = \frac{-c}{\omega L}\Delta\Phi \ . \qquad (16)$$

The calibration between phase shifts and the output voltage of the phase-locked loop was simply a matter of changing the signal synthesizer phase by a known amount relative to the reference and recording the change in the phase-locked-loop voltage.

A third calibration measured the undesired effect of the signal amplitude on the output of the phase measurement system. This effect was assumed to be linear in the amplitude of the signal. The resulting correction required was a maximum of $\sim 10\%$ at the lowest pressure and significantly less at higher pressures.

The deconvoluted data plots typically exhibit a knot of points at T_{c1}. This represents the normal liquid points which, due to the absence of a real NMR shift above T_{c1}, were compressed into the region near T_{c1}.

As a final note, no effects (due to the nature of ^{3}He or otherwise) caused by coupling of the NMR and the sound were ever noticed. Tewordt and Schopohl[27] have studied this possibility theoretically.

V. RESULTS AND INTERPRETATIONS

For all of the runs, the applied field $\hat{H}$ was parallel to the sound vector $\hat{q}$. Ideally this should limit the axis of the order parameter $\hat{l}$ to lie in the plane perpendicular to $\hat{H}$ and $\hat{q}$. Since the sound dispersion should depend only on $\hat{l}\cdot\hat{q}$, the theoretical results calculated for the perpendicular components of the attenuation and velocity shift should apply.

To date, the only quantitatively successful attempt at fitting experimental A-phase sound data is a series of rather involved numerical calculations for 24, 26, and 33.5 bars.[28] We cannot say at this time if this scheme would fit our data. Certainly, it cannot be directly applied to the A_1 phase as Wölfle and Koch assume zero magnetic field. Instead, we will use the collisionless theory[4] as a guide for comparing the results between pressures. The Ginzburg-Landau result for the magnitude of the energy gap will be assumed here,

$$\left[\frac{\Delta}{k_B T_c}\right]^2 = \frac{2\pi^2}{3}\left[\frac{\Delta C}{C_N}\right](1 - T/T_c) \ , \qquad (17)$$

where it is hoped that all strong-coupling effects are accounted for by the experimentally measured heat-capacity jump at T_c, $(\Delta C/C_N)$.

A. Attenuation

The qualitative features common to our reduced attenuation data from the five pressures and three field magnitudes can be seen in the example of Fig. 6. The warm side of the clapping maximum is considerably steeper than the cold side and exhibits a hump in the A_1 phase which would have developed into a separate peak if the field strength had been increased several times. The relative placement of T_{c1} and T_{c2} are determined by the choice $\delta = 0.25$. The increased scatter of the points in the A_1 phase is because the slope of the NMR shift used for thermometry is only one-fifth of that in the A phase.

The simplest characterization of the A-phase attenuation data is made by a list of the heights and temperatures of the maximum attenuation peaks. Since no significant systematic variation of those quantities as a function of magnetic field strength was seen, average values at each pressure can lump the 14-, 29-, and 42-mT data together.

The collisionless theory says that the sound attenuation should be

$$\alpha_0 = \frac{\hbar\omega^2}{c_0 F_0^s k_B T_c}\,\mathrm{Im}(\mathcal{X}) \ , \qquad (18)$$
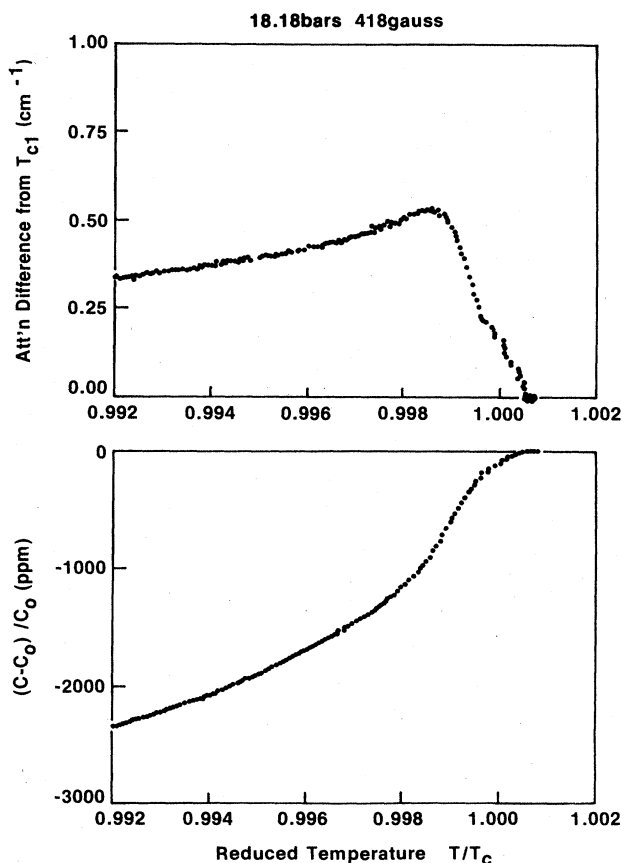

FIG. 6. Data example taken at 18.18 bars in a field strength of 41.8 mT. The width of the A_1 phase can be seen by the "shoulder" in the attenuation and the decreased velocity slope.

where $\mathcal{X}$ is a universal function of $(\Delta_0/\hbar\omega)$ only. For the ABM state, the gap maximum is $\Delta_0 = (3/2)^{1/2}\Delta$. If one interprets the maximum attenuation peak at each pressure as being caused by the same value of $\mathcal{X}$ [e.g., $\mathcal{X}(1/1.23)$ for the clapping mode] then the heights of these peaks should scale as the prefactor of $\mathcal{X}$ in Eq. (18). We find that our peak heights, as well as those from earlier high-pressure A-phase studies, do indeed scale as Eq. (18). Figure 7 shows these data plotted as a function of pressure (higher-frequency data are scaled by $[(f(\text{MHz})/5]^2)$ and compared against Eq. (18) multiplied by $\frac{1}{4}$. This arbitrary value was chosen since the theoretical curve lies far too high otherwise. Smearing out of the attenuation peaks due to the finite average quasiparticle lifetime might explain some lowering of the 5-MHz high-pressure attenuation peaks, but probably not much more than the difference between the 5-MHz and 15- and 20-MHz data.

If the attenuation peak maximum is indeed due to the clapping resonance, then T/T_c for this peak should result from inserting $\hbar\omega = 1.23\Delta_0$ into Eq. (17). Figure 8 is a plot of this theoretical value and the experimental results versus pressure. The agreement is not good, especially at high pressures. From the numerical plots in Wölfle and Koch,[28] the location of the $\alpha_\perp$ peak is apparently little affected by the inclusion of dissipation. For this reason, quasiparticle lifetime effects may not explain the peak location discrepancy. Problems with input data for the thermometry calibration could be suspect, but it should be noted that corrections to $(\Delta C/C_N)$ or $k_B T_c$ shifts both the experimental and theoretical points in the same direction. Another possibility is that specular reflection in the sound cell significantly mixes in the attenuation components important for $\hat{l}\cdot\hat{q}\neq0$. For example, the peak in

FIG. 8. Temperature locations of the clapping peaks as a function of pressure.

α_c occurs at a temperature 2.4 times colder than the $\alpha_\perp$ peak due to clapping. The data of Paulson et al.[8] also show 5-MHz attenuation peaks which occur at temperatures lower than predicted. Their lesser discrepancy can be chiefly attributed to a difference in temperature scales.

B. Phase velocity changes

The rate at which the sound velocity drops below T_c from its normal liquid value increases by roughly a factor of 2 on going from our highest pressure (31 bars) to the lowest pressure at which a velocity measurement was made (9 bars). The low-temperature limit of this velocity drop is expected on theoretical grounds to be the first sound velocity c_1. However, an attempt to scale the velocity runs by $(c_0-c_1)/c_0$ did not work very well. Turning again to the collisionless theory for superfluid sound dispersion, the velocity change near T_c is seen to be proportional to the gap for T near T_c:

$$\frac{c-c_0}{c_0} \propto \frac{\Delta(T)}{F_0^s k_B T_c} . \tag{19}$$
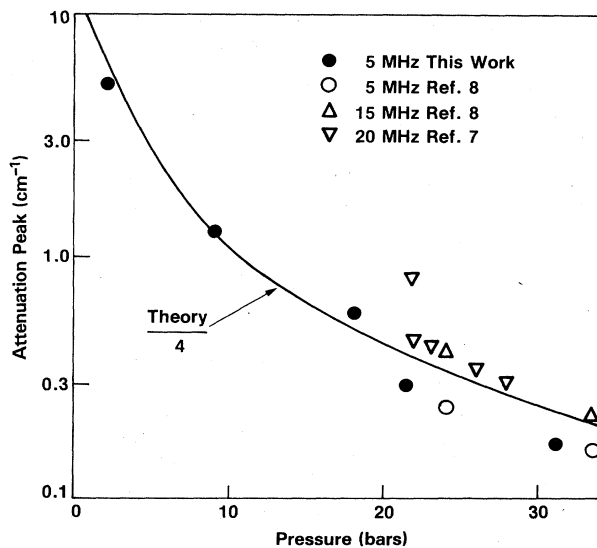
This suggests a scaling by the factor

FIG. 7. Clapping attenuation peak magnitudes as a function of pressure. For comparison, data at higher frequencies are scaled by $[f(\text{MHz})/5]^2$ and the theoretical curve is divided by the arbitrary factor of 4.
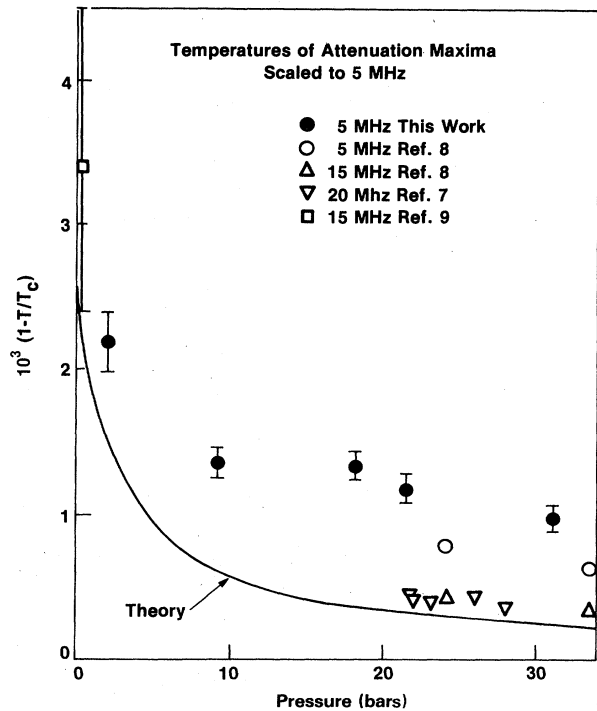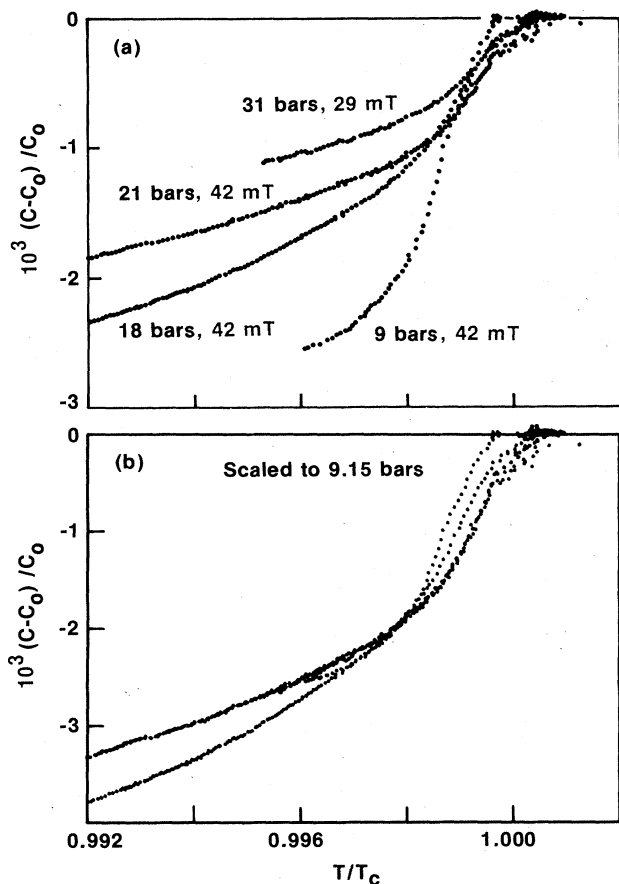
FIG. 9. Velocity shift plots from the coldest run at each pressure. (b) is the same as (a) but with each run scaled by the pressure-dependent factor of Eq. (20) to 9.15 bars.

$$\frac{\Delta}{F_0^s k_B T_c (1 - T/T_c)^{1/2}} \propto \frac{(\Delta C/C_N)^{1/2}}{F_0^s} . \tag{20}$$

Figure 9 shows that such a scaling is approximately valid.

The shape of the velocity-versus-temperature curves is qualitatively different from the zero-sound picture, which predicts exactly zero shift in the velocity for temperatures above the pair breaking limit $\hbar\omega = 2\Delta$. Although the shape of the velocity curves initially suggests it, fitting the curves to a constant times $(1 - T/T_c)^{1/2}$ was not successful. For lower-temperature data $\hbar\omega \ll \Delta$, where the velocity is expected to go as the viscosity, such fits might be possible. The lowest pressure data at 9 bars seem to suggest relatively little drop in the velocity in the A_1 phase.

VI. CONCLUSION

Measurements of the velocity and attenuation of 5-MHz sound have been presented. This frequency was chosen so that, in the A_1 and A phases of ^{3}He just below T_c, the period of oscillation of the sound is much shorter than the quasiparticle collision time τ ($\omega\tau \gg 1$), while at the same time the energy of the sound quantum $\hbar\omega$ is much lower than the thermal energy ($\hbar\omega \ll k_B T_c$). This allowed the most valid comparison to the analytic theory. Although the temperature and frequency dependences of the theory had been shown to be approximately valid at high pressure, these measurements, performed down to a pressure of 2 bars, show that the pressure dependences of the height of the attenuation maximum and the rapid velocity drop (just below T_c) are qualitatively correct. It does not appear that inclusion of finite quasiparticle lifetime effects can account for the differences between the theory and the data. Although the change is small, the velocity does begin to drop as soon as one cools into the A_1 phase, contrary to the prediction that the velocity remains temperature independent until $\hbar\omega = 2\Delta$. The precision of these measurements depends greatly on the *in situ* NMR thermometry. This precision technique will be useful in future measurements on the A and A_1 phases of ^{3}He.

*Present address: Thermophysics Division, National Bureau of Standards, Gaithersburg, MD 20899.

[1]Theoretical reviews of superfluid ^{3}He have been written by A. J. Leggett, Rev. Mod. Phys. **47**, 331 (1975); P. W. Anderson and W. F. Brinkman, in *The Physics of Liquid and Solid Helium, Part 2*, edited by K. H. Benneman and J. B. Ketterson (Wiley, New York, 1978), p. 177; P. Wölfe, Rep. Prog. Phys. **42**, 269 (1979). Experimental reviews are J. C. Wheatley, Rev. Mod. Phys. **47**, 415 (1975); J. C. Wheatley, in *Progress in Low Temperature Physics*, edited by D. F. Brewer (North-Holland, New York, 1978), Vol. 7A; and D. M. Lee and R. C. Richardson, in *The Physics of Liquid and Solid Helium, Part 2*, edited by K. H. Benneman and J. B. Ketterson (Wiley, New

York, 1978), p. 287.

[2]J. W. Serene, Ph.D. thesis, Cornell University, 1974 (unpublished).

[3]P. Wölfe, Phys. Rev. Lett. **30**, 1169 (1973).

[4]P. Wölfe, in *Progress in Low Temperature Physics*, edited by D. F. Brewer (North-Holland, New York, 1978), Vol. 7A.

[5]D. N. Paulson, R. T. Johnson, and J. C. Wheatley, Phys. Rev. Lett. **31**, 746 (1973).

[6]D. T. Lawson, W. J. Gully, S. Goldstein, R. C. Richardson, and D. M. Lee, Phys. Rev. Lett. **30**, 541 (1973); J. Low Temp. Phys. **15**, 169 (1974).

[7]J. B. Ketterson, P. R. Roach, B. M. Abraham, and P. D. Roach, in *Quantum Statistics and the Many-Body Problem*,

edited by S. B. Trickey, W. P. Kirk, and J. W. Dufty (Plenum, New York, 1975).

[8]D. N. Paulson, M. Krusius, and J. C. Wheatley, J. Low Temp. Phys. **26**, 1973 (1977).

[9]O. Avenel, L. Piche, and E. Varoquaux, Physica **107B**, 689 (1981).

[10]G. F. Spencer, P. W. Alexander, and G. G. Ihas, Cryogenics **22**, 167 (1982).

[11]D. D. Osheroff, W. J. Gully, R. C. Richardson, and D. M. Lee, Phys. Rev. Lett. **29**, 920 (1972); D. D. Osheroff, R. C. Richardson, and D. M. Lee, *ibid.* **28**, 885 (1972).

[12]R. C. Richardson, Physica **90B**, 47 (1977).

[13]A. J. Leggett, Phys. Rev. Lett. **29**, 1227 (1972).

[14]A. J. Leggett, Ann. Phys. (N.Y.) **85**, 11 (1974).

[15]D. D. Osheroff and P. W. Anderson, Phys. Rev. Lett. **33**, 686 (1974).

[16]R. A. Webb, R. E. Sager, and J. C. Wheatley, Phys. Rev. Lett. **35**, 615 (1975); **35**, 1164 (1975); W. P. Halperin, C. N. Archie, F. B. Rasmussen, T. A. Alvesalo, and R. C. Richardson, Phys. Rev. B **13**, 2124 (1976).

[17]A. I. Ahonen, M. Krusius, and M. A. Paalanen, J. Low Temp. Phys. **25**, 421 (1976).

[18]R. W. Giannetta, Ph.D. thesis, Cornell University, 1980, unpublished

[19]R. F. Berg, B. N. Engel, and G. G. Ihas, in *Proceedings of the 17th International Conference on Low Temperature Physics,* edited by U. Eckern, A. Schmid, W. Weber, and H. Wühl (North-Holland, Amsterdam, 1984), p. 1171.

[20]B. N. Engel, R. F. Berg, and G. G. Ihas (unpublished).

[21]S. Takagi, J. Low Temp. Phys. **18**, 309 (1975).

[22]N. D. Mermin and G. Stare, Phys. Rev. Lett. **30**, 1135 (1973).

[23]T. A. Alvesalo, T. Haavasoja, and M. T. Manninen, J. Low Temp. Phys. **45** 373 (1981).

[24]D. C. Sagan, P. G. N. deVegvar, E. Polturak, L. Friedman, S.-S. Yan, E. L. Ziercher, and D. M. Lee, Phys. Rev. Lett. **53**, 1939 (1984).

[25]U. E. Israelsson, B. C. Crooker, H. M. Bozler, and C. M. Gould, Phys. Rev. Lett. **53**, 1943 (1984).

[26]W. P. Halperin, C. N. Archie, F. B. Rasmussen, T. A. Alvesalo, and R. C. Richardson, Phys. Rev. B **13**, 2124 (1976).

[27]L. Tewordt and N. Schopohl, J. Low Temp. Phys. **34**, 489 (1979).

[28]P. Wölfle and V. E. Koch, J. Low Temp. Phys. **30**, 61 (1978).